Shipborne MAX-DOAS Observations of Tropospheric Trace Gases over a Coastal City and the Yellow Sea near Qingdao, China

XIANXIN LI, ZHANGJUN WANG, LIBIN DU, XINGTAO LIU, XIUFEN WANG, CHAO CHEN, XIANGQIAN MENG, HUI LI, QUANFENG ZHUANG, WEI DENG, AND XIN PAN

Institute of Oceanographic Instrumentation, Qilu University of Technology, Shandong Academy of Sciences, Shandong Provincial Key Laboratory of Ocean Environmental Monitoring Technology, Qingdao, China

XINZHAO CHU

Cooperative Institute for Research in Environment Sciences, and Department of Aerospace Engineering Sciences, University of Colorado Boulder, Boulder, Colorado

(Manuscript received 9 October 2018, in final form 28 December 2019)

ABSTRACT

Observations of the atmospheric trace gases are crucial for quality assessment of the human living environment. Multiaxis differential optical absorption spectroscopy (MAX-DOAS) is the most promising candidate to meet the requirements on observations of atmospheric trace gases with high sensitivity, good stability, and a wide range of regional monitoring. The shipborne observations of tropospheric trace gases (NO_2, SO_2, and O_3) over a coastal city, Qingdao, with MAX-DOAS were conducted by a Chinese oceanographic research vessel, *XiangYangHong 08* (*XYH 08*). During the observational campaign, the shipborne MAX-DOAS equipment was used to make anchor measurements for 3 days, and a sailing measurement along Qingdao coast for half an hour. Measurement results are presented for both sailing and anchor point measurements in this paper. Combining geometry characteristic of the monitoring area, it can be concluded from the sailing measurements that the traffic emissions may play an important role in the boundary layer (BL) pollution of a coastal city's atmosphere. The anchor point measurements showed that the NO_2 vertical column density (VCD) mean value of Jiaozhou Bay is about 2.7 times of the value of the Qingdao offshore sea area. Likewise, the tropospheric VCDs of SO_2 and O_3 have an increase of 30% and 40%, respectively, on 1 September in Jiaozhou Bay, compared to the other 2 days in Qingdao offshore sea area.

1. Introduction

The "health" of Earth's atmosphere is one of the greatest societal concerns today, especially urban air quality. Air pollution, in the forms of aerosols (such as smog) and trace gases (such as industrial emission), poses serious threats to human health, causes plant damage, and induces other environmental problems (Khalil and Rasmussen 1990; Schempp et al. 2004; Platt and Stutz 2008). Resolving and mitigating these environmental issues demand a sound scientific understanding of the fundamental physical and chemical processes involving the atmospheric compounds, and an accurate quantification of the trace gases and aerosols in the atmosphere. In particular, atmospheric trace gases have multiple impacts: Greenhouse gases, such as CO_2, H_2O, and CH_4, are key factors to climate change, while polluting gases, such as NO_2, SO_2, and O_3, affect air quality. Therefore, accurate determination of trace gas species and concentrations is crucial to environmental quality assessment and climate research.

However, simultaneous measurements of multiple trace gases are still great technological challenges for the society, although numerous methods have been developed over the last many decades. The in situ analyzers can make simultaneous point measurements of multiple trace gases but cannot cover large areas unless if such a device is installed in commercial airlines (Machida et al. 2008). The differential absorption lidar (DIAL) equipment provides the trace gas range-resolved profile with good signal-to-noise ratio (SNR) when compared with

Corresponding author: Zhangjun Wang, zhangjun.wang@hotmail.com

DOI: 10.1175/JTECH-D-18-0179.1

passive remote sensing techniques (Edner et al. 1994); however, it is difficult for conventional DIALs to measure simultaneously multiple trace gas species, and the measurement accuracy is limited due to interference gases. High-precision measurements of trace gases can be made by tunable diode-laser absorption spectroscopy (TDLS) method, but the tunable diode-laser technology is still quite complex and the laser diodes optimized for spectroscopic purposes, especially in the visible and ultraviolet spectral ranges, are still difficult to obtain (Platt and Stutz 2008). The Fourier transform infrared (FTIR) spectroscopy method is a good application of infrared spectrum in trace gas measurements but the cost of such an IR spectrometer is high (Bertschi et al. 2003).

Compared to the above approaches, the differential optical absorption spectroscopy (DOAS) possesses several advantages as it can make simultaneous and long-range measurements of multiple trace gases through hundreds of spectral channels (Platt 1994). Because of its very long optical path, DOAS exhibits very high sensitivity thus can detect species with extremely weak absorption features (Platt and Stutz 2008). The DOAS measurements are classified into two main types: active DOAS and passive DOAS. The active DOAS utilizes artificial light sources (such as a xenon lamp with a broad spectrum) to observe multiple trace gases simultaneously, which requires much more sophisticated optical systems, more maintenance, and more power than passive instruments (Platt 1994). On the other hand, the passive DOAS technique can be deployed in two different configurations: measuring zenith sky-scattered radiation by pointing the radiation input of the spectrometric system toward the zenith or measuring the radiation reaching the spectrometric system for directions away from the zenithal one. This last configuration is usually called multiaxis DOAS (MAX-DOAS) and it allows for measurements of the tropospheric trace gases near the ground surface over a large range with much simpler instrument structures and less maintenance than the active DOAS device. This is why the passive DOAS has been found wide applications in recent years. Off-axis DOAS observations were first made by Sanders et al. (1993) to observe OClO over Antarctica during the twilight in 1993 aiming to increase the measurements sensitivity in the lower absorption layers. MAX-DOAS was proposed by Hönninger et al. (2004) to observe tropospheric trace gases combined with multiple scattering radiative transfer modeling. Since then, the MAX-DOAS technique has become popular for assessing the column densities of tropospheric trace gases utilizing multiple-angle observations of scattered sunlight (Heckel et al. 2005; Leigh et al. 2006; Wittrock et al. 2003).

Among the various platforms for MAX-DOAS deployment, the shipborne MAX-DOAS, despite exhibits challenges due to the shaking of the ship, presents distinct advantages over the vehicle-based DOAS, especially for the tropospheric trace gas measurements in coastal urban areas. As the dense buildings shelter sunlight in off-axis angles in the urban areas, the vehicle-based passive DOAS only gives reliable measurements in the zenith direction, which is more sensitive to the trace gases in the stratosphere than in the troposphere unless for the flux measurement of a point source (Galle et al. 2003) or total emission quantification of a megacity (Johansson et al. 2008). These studies were mainly focused on the tropospheric heavy pollution measurements under the assumption that the stratospheric trace gas absorption have almost no change due to the relative constant solar zenith angle (SZA) during the short measurement time. The shipborne MAX-DOAS can overcome the limitations of vehicle-based passive DOAS for coastal cities because the sufficient long distance between the ship and a coastal city enables the MAX-DOAS to measure the tropospheric trace gases near the urban ground surface with high sensitivities. Although several shipborne DOAS observations have been reported in literatures, for example, volcanic SO_2 by Edner et al. (1994) and Weibring et al. (1998, 2002), the bromine monoxide in a volcanic plume by Bobrowski et al. (2003), BrO and NO_2 in the marine troposphere by Leser et al. (2003), and NO_2 over the western Pacific and Indian Ocean by Takashima et al. (2012), most of these observations were made over the open water in the ocean and few shipborne observations have been reported over a coastal city (Premuda et al. 2011).

In this paper, we report the MAX-DOAS observations of multiple tropospheric trace gases (NO_2, SO_2, and O_3) over a coastal city—Qingdao, China—during a research campaign in late August 2014. A MAX-DOAS system was deployed on a research vessel that sailed several to tens of kilometers off the shore. Such long distance allowed the MAX-DOAS equipment to point toward the coastal city at very low elevation angles (e.g., 5°–10°), enabling the sensitive measurements of trace gases near the ground in the urban area of Qingdao. Figure 1 illustrates the scenario of the shipborne MAX-DOAS measurements of a coastal city, where different types of scattering events and different light paths are indicated. More details about the observational campaign and the MAX-DOAS instrument are introduced in section 2, while the MAX-DOAS measurement principles and data retrieval procedures are outlined in section 3. We then present the observational results and discussions in section 4 and the conclusions of this work are introduced in section 5.

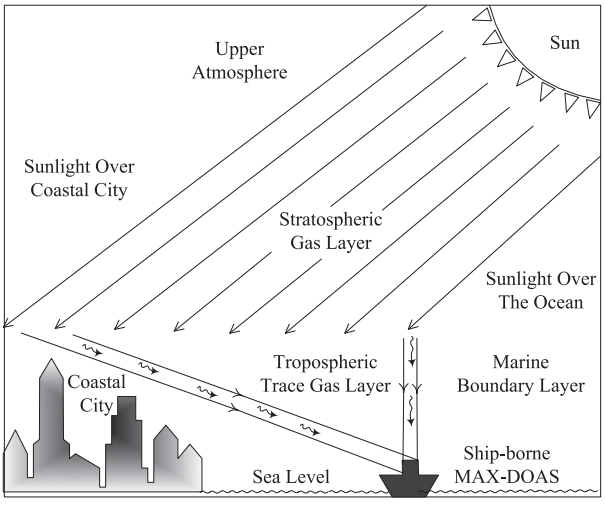

FIG. 1. Scenario for shipborne MAX-DOAS measurements of the coastal city.

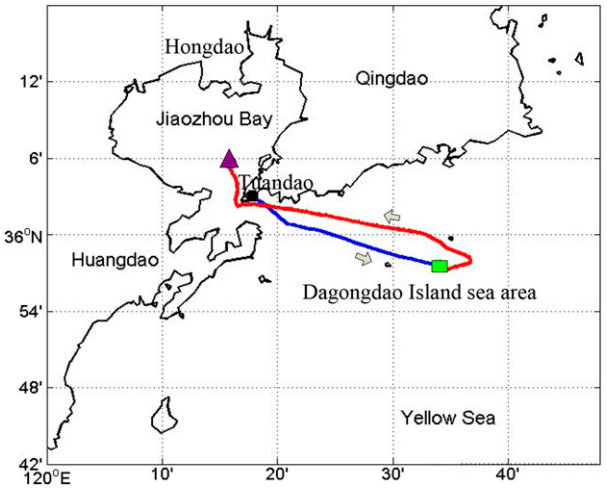

FIG. 2. Map and sailing route of the shipborne observational campaign.

2. Observational campaign and MAX-DOAS instrumentation

a. *Shipborne MAX-DOAS observational campaign along the coastal city*

The shipborne observation campaign was conducted by the Chinese oceanographic research vessel, *XiangYangHong 08* (*XYH 08*; see Fig. 4), from Jiaozhou Bay to Dagongdao Island along the coastal city, as illustrated in Fig. 2. The research ship started from Tuandao Island (the circular dot in Fig. 2) at 0750 local time (LT; LT = UTC + 8 h) 30 August 2014, sailed along the shore of Qingdao (The curve of the lower position in Fig. 2), and reached the anchor spot (the rectangle spot in Fig. 2, 35.9602°N, 120.5665°E) near Dagongdao Island (~6 km located southeastern of Dagongdao Island) at 0930 LT. The shipborne MAX-DOAS was running to make sailing measurements toward Qingdao during this sailing route, and the details will be discussed in section 4b. Then the shipborne MAX-DOAS carried out measurements for 2 days at the first anchor spot, and the details will be discussed in section 4c. The research ship sailed from the first anchor spot via the second route (the curve of the upper position in Fig. 2) to the second anchor spot (the triangular spot in Fig. 2, 36.0942°N, 120.2651°E) located in Jiaozhou Bay at 1900 LT 31 August 2014. Because it was night, shipborne MAX-DOAS measurements were not performed during this sailing route. The vessel reached the second anchor spot at 2030 LT 31 August and then stayed there, where the shipborne MAX-DOAS made continuous measurements until 2 September. The research ship returned to Qingdao port on 2 September 2014, and completed the 3-day observation campaign.

b. *Shipborne MAX-DOAS instrument design*

The instrument used in the shipborne trace gases measurements is a MAX-DOAS system with an inclinometer recording the ship posture and an electronic compass recording the azimuth angle. This system consists of the telescope, the spectrometer (spectral range is 290–420 nm, resolution is better than 0.4 nm), the scanner, the light collection window, the temperature control system, the optical fiber, and the control computer. The instrumental structure is shown in Fig. 3. The telescope is 50.8 mm in diameter and 150 mm in focus length. The receiving telescope collects the sky scattered sunlight that travels through absorbers like atmospheric trace gases. The scanner turns the receiving telescope to multiple elevation angles (5°, 10°, 20°, and 90° elevation angle for a complete measurement sequence). Light collection window was installed on the top of the instrument for light transmission. The temperature control system is used to provide a constant temperature environment at 20° for the spectrometer with a precision better than 1°. The thermoelectric cooling devices (TEC) were used for the temperature cooling.

3. DOAS/MAX-DOAS methods, spectral data processing, and trace gases concentration retrievals

The retrieval of atmospheric trace gases column densities with the MAX-DOAS technique is based on the DOAS method. Briefly, the DOAS method for the zenith sky configuration utilizes a modified version of the Lambert–Beer extinction law where the log-ratio of two spectra measured for different SZAs—usually the reference spectrum is obtained at noon—is subtracted

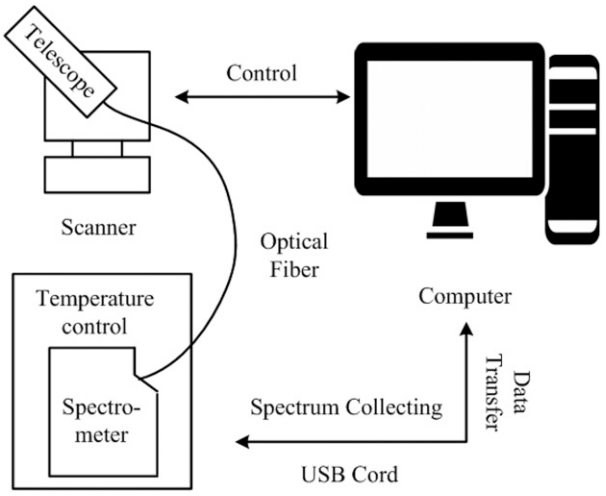

FIG. 3. Functional sketch of the shipborne MAX-DOAS system.

from its mean function giving a differential quantity usually called differential optical density (DOD). The mean function can be calculated with a high-pass-filter procedure based on the fast Fourier transform (FFT) (Bortoli et al. 2009b) or with a low-order polynomial fitting (Platt 1994). The DOD is then fitted with the differential cross sections (DCS) on the UV–visible spectral region of the absorbers under investigation obtained with the same process above described. The outputs of the DOAS method are the integrated trace gas concentrations along the absorption path usually called slant column densities (SCDs). Actually, due to the differential features, the selected SCD is the differential SCD (DSCD), meaning that it is the difference in terms of absorber content, between the reference spectrum and the analyzed one. Therefore, the actual slant column density (ASCD) is the DSCD plus the trace gas amount in the reference spectrum (SCDref). This last value, for midlatitudes, can be calculated with a Langley plot of the DSCD diurnal series toward airmass factor (AMF) that is the geometrical correction factor function mainly of SZA and wavelength that let to determine the total column or vertical column density (VCD) of the considered tracer. The AMF is calculated with radiative transfer models (Hönninger et al. 2004; Hendrick et al. 2006). In summary, for a zenith sky configuration, the measurements are performed in a fixed direction (zenith) and the variation of the SZAs and consequently of the AMFs allows for the determination of the tracer's VCDs. Further application of inversion's method allows for the retrieval of the vertical distribution of some tracers (Bortoli et al. 2009a). On the other hand, in the MAX-DOAS technique, the SZA is assumed to be constant along the measurements for different elevations of the radiation input and the zenith measure is considered as the reference one for each measurement cycle. In this situation the output of the DOAS algorithms can be considered as the sum of the stratospheric and of the tropospheric DSCD. Assuming constant the stratospheric absorber's content and processing the measurements carried out at local noon, the difference of the DSCDs gives the content of the selected absorber in the troposphere. For the retrieval of the tropospheric VCD, we follow the methods described in Ma et al. (2013).

a. Retrieval of trace gases $SCD_{\alpha,total}$ by DOAS analysis

The spectral structure and radiation intensity of the incident sunlight at the top of the atmosphere (TOA) will change when passing through the atmosphere because of the absorption and light extinction of different atmospheric compounds. The sunlight intensity $I(\lambda)$ received by the detector at the surface, following the Lambert–Beer law, is

$$I(\lambda) = I_0(\lambda)\exp\left\{-\sum_{j=1}^{n}\left[\sigma_j(\lambda)\int_0^l c_j(l)\,dl\right]\right\}, \qquad (1)$$

where, $I_0(\lambda)$ is the intensity of the incident sunlight at TOA, $\sigma_j(\lambda)$ is the absorption cross section of the jth atmospheric molecule [absorption cross sections of NO_2, SO_2, and O_3 used in this paper are from Bogumil et al. (2003)], $c_j(l)$ is the concentration of the jth trace gas species in the atmosphere, l is the optical pathlength when incident sunlight pass through the atmosphere. The effect of Rayleigh and Mie scattering can be removed by a low-order polynomial procedure. Applying the log to both sides of Eq. (1), and then applying the high-pass-filtering algorithm to both sides of Eqs. (1) and (2) could be obtained as

$$\left[\ln\left\{\frac{I(\lambda)}{I_0(\lambda)}\right\}\right]' = -\sum_j \sigma_j'(\lambda)\mathrm{SCD}_j, \qquad (2)$$

where the slant column density $\mathrm{SCD}_j = \int_0^l c_j(l)\,dl$ is the integration of the concentration of the jth trace gas species along the light path through the atmosphere, and $[\ln\{I(\lambda)/I_0(\lambda)\}]'$ is the differential absorption optical density dealt by a filtering procedure. Then the slant column density (SCD_j) can be obtained by a fitting algorithm between the differential absorption optical densities and differential absorption cross sections of specific trace gases. The total $\mathrm{SCD}_{\alpha,\mathrm{total}}$ can be expressed as the sum of a tropospheric part and a stratospheric part (Ma et al. 2013):

$$\mathrm{SCD}_{\alpha,\mathrm{total}} = \mathrm{SCD}_{\mathrm{trop}} + \mathrm{SCD}_{\mathrm{strat}}. \qquad (3)$$

The SCD errors of the DOAS fitting process mainly come from sources such as interference gases, spectrum

noise and spectral shift, absorption cross section of trace gases, removal of Fraunhofer bands, spectrometer stray light, and offsets. The interference of other trace gas absorptions can cause the contamination of the absorption cross sections (Platt and Stutz 2008), which will influence the accuracy of absorption cross section and produce the systematic error. The electrical noise of the spectrometer detector can affect the final DOAS fitting results. In our measurement, it was minimized by averaging 100 adjoin individual spectrums to record one spectrum consuming several tens of seconds sampling time according to the weather condition. The temperature variation of the environment can cause change of the absorption cross sections of the trace gases. So the variations of trace gases absorption cross sections due to the temperature variation in the atmosphere environment can cause the uncertainty of fitting results. It will influence the precision and accuracy of the results. The spectral shift produced by the spectrometer was reduced with its thermoregulation (20° ± 1°C).

The WinDOAS is a program developed for DOAS analysis with a friendly user interface and some powerful DOAS tools. The WinDOAS program, extensively validated by many different campaigns, has already been used worldwide and for many different DOAS applications. To make error estimation of our shipborne MAX-DOAS measurements, we use WinDOAS to analyze the spectrum data. The SCD errors of the respective trace gases are evaluated by the standard deviations of the fitted parameters (SCD of various species) calculated by the WinDOAS. In the DOAS fitting mode of the WinDOAS, a Marquardt–Levenberg nonlinear least squares (NLLS) algorithm will be used in the spectrum data analysis. NLLS method includes a gradient-search algorithm (Bevington and Robinson 1992), which is based on the iterative combination of a steepest-descent method and a linearization of the fitting function, and a singular value decomposition (SVD) method (Press et al. 1992), a kind of linear least squares (LLS) fit algorithm. The standard deviations are calculated directly from the SVD algorithm and from the Marquardt–Levenberg algorithm in data retrieval process analyzed by the WinDOAS. All the error bars showed in the results and discussion section are represented by the standard deviations of the fitted parameters analyzed by the WinDOAS under the DOAS fitting mode.

b. *Calculation of "tropospheric differential" slant column density ($DSCD_{\alpha,trop}$)*

The last scattering event mostly takes place in the lower troposphere. As a result, the last scattering altitude (LSA) for zenith view direction is below 5 km according to the aerosol loading and atmosphere visibility (Hönninger et al. 2004, their Fig. 8). If the trace gases such as NO_2 is mainly distributed near the ground, for example, 1–2 km, and considering that the last scattering events mostly take place in the near-surface troposphere, the light path traveling through the stratosphere is independent from the telescope elevation angle. Consequently, the stratospheric tracer SCDs of the α elevation angle (not zenith-view direction) are nearly equal to the stratospheric SCDs of the 90° elevation angle (zenith-view direction) for each cycle of MAX-DOAS measurements at different viewing elevations. Thus, we can make the approximation as shown in Eq. (5). As a result, the variations of stratospheric trace gas concentrations during one measurement cycle are ignored. Thus, the approximation actually introduces inevitable error:

$$\mathrm{SCD}_{\alpha,\mathrm{strat}} \approx \mathrm{SCD}_{90^\circ,\mathrm{strat}}. \tag{4}$$

The Fraunhofer reference spectrum (FRS) is a reference spectrum used in retrieval process, including the Fraunhofer structure of the solar spectrum. The FRS can be divided into two types according to the following two approaches. The so-called fixed FRS is the spectra obtained at the 90° elevation angle under small SZA (at local noon). And the so-called current cycle FRS is the spectra obtained at 90° elevation angle in each cycle of the MAX-DOAS measurement. The DSCD of the analyzed compound is obtained with the DOAS algorithms [Hönninger et al. 2004, their Eq. (3)]. When the FRS is applied to retrieve the measured spectra, the FRS also contains atmospheric trace gas absorption. The DSCD represents the difference in absorption between the measured atmospheric spectra and the FRS (Ma et al. 2013). In this paper, the differential slant column density of tropospheric trace gases ($\mathrm{DSCD}_{\alpha,\mathrm{trop}}$) was obtained by analyzing the scattered solar spectrum measured in the zenith and off-axis directions (e.g., α) under the current cycle FRS measurement case using the DOAS retrieval method. The deduction of the stratospheric trace gas SCD is based on the ideal scattering model that assumes the same light path traveling through the stratosphere between zenith observed spectrum and off-axis observed spectrum. In high aerosol loads or cloudy conditions, the uncertainty of the approximation will increase inevitably. Moreover, the stratospheric trace gas concentrations are assumed to be constant in the zenith and off-axis observation modes. However, during the period of a measurement cycle, the zenith spectrum was measured several minutes behind the off-axis spectrum. So the spatial and temporal variety of stratospheric trace gases over the measurement period was ignored, which inevitably introduced uncertainties. The error determined

by stratospheric SCD is intrinsic especially for high aerosol loads or cloudy conditions, which cannot be removed by statistical method. In our measurements, the error of the retrieved ''tropospheric differential'' slant column density (DSCD) is estimated to be low for trace gases, considering low aerosol loads during measurements and the very short time interval between zenith and off-axis measurement in the current cycle measurement case.

c. *Deduction of tropospheric trace gases vertical column density (VCD_{trop})*

Since the SCD depends on the elevation angle of specific measurement, it should be converted into the VCD that does not depend on the specific elevation angle. As a result, we can evaluate different MAX-DOAS measurements by VCD comparison. The VCD can be calculated by slant column density and AMF. The AMF can be defined as

$$\mathrm{AMF}(\lambda,\theta,\alpha,\phi)=\frac{\mathrm{SCD}(\lambda,\theta,\alpha,\phi)}{\mathrm{VCD}}, \tag{5}$$

where θ is the solar zenith angle, α is the elevation angle of telescope, ϕ is the relative azimuth angle between the solar azimuth and telescope direction, and λ is the light wavelength. As a result, Eq. (5) can be rewritten as

$$\begin{aligned}\mathrm{DSCD}_{\alpha,\mathrm{trop}} &= \mathrm{SCD}_{\alpha,\mathrm{trop}}-\mathrm{SCD}_{90^\circ,\mathrm{trop}}\\ &= \mathrm{VCD}_{\mathrm{trop}}\mathrm{AMF}_{\alpha,\mathrm{trop}}-\mathrm{VCD}_{\mathrm{trop}}\mathrm{AMF}_{90^\circ,\mathrm{trop}}\\ &= \mathrm{VCD}_{\mathrm{trop}}(\mathrm{AMF}_{\alpha,\mathrm{trop}}-\mathrm{AMF}_{90^\circ,\mathrm{trop}})\\ &= \mathrm{VCD}_{\mathrm{trop}}\mathrm{DAMF}_{\alpha,\mathrm{trop}}.\end{aligned} \tag{6}$$

The DAMF is the so-called differential tropospheric airmass factor. Considered that most of the light is scattered above the boundary layer (Leser et al. 2003) and the trace gases are mainly located in the boundary layer, under the single scattering approximation circumstance, the AMF can be expressed by geometry approximation as

$$\mathrm{AMF}_{\alpha,\mathrm{trop}}=\frac{1}{\sin(\alpha)}, \tag{7}$$

where α is the telescope elevation angle (Wagner et al. 2010). As a result, with geometry approximation $\mathrm{AMF}_{90,\mathrm{trop}}=1$ (Ma et al. 2013), from Eq. (6) the $\mathrm{VCD}_{\mathrm{trop}}$ can be obtained by

$$\mathrm{VCD}_{\mathrm{trop}}=\frac{\sin(\alpha)\mathrm{DSCD}_{\alpha,\mathrm{trop}}}{1-\sin(\alpha)}. \tag{8}$$

AMF can be further calculated by atmospheric radiation transfer model. In this paper, AMF is calculated with SCIATRAN, a kind of comprehensive radiation transfer model considered multiple scattering effect (Rozanov et al. 2005). Different atmospheric radiative transmission conditions, such as aerosol, cloud, surface albedo, and profiles of the absorbers, can influence the calculation of the AMF (Hönninger et al. 2004). So in our measurement, the different atmospheric radiative transmission parameters used in the SCIATRAN RTM contributed a lot to the uncertainties of the results of the AMF. Although the shipborne MAX-DOAS measurements were made on the sea, the measurement site is very close to the shoreside and the sailing measured trace gases are mostly distributed over the coastal city. So the same conditions were approximated with ground-based situations for the radiative transfer model of the shipborne MAX-DOAS. The minor ship vibrations were ignored due to the good sea conditions during the 3-day shipborne MAX-DOAS measurements (see section 3d). However, the small ship vibration could cause a small elevation angle error for the MAX-DOAS observation, which inevitably introduced some uncertainties of the AMF result. The error caused by the AMF calculation in the MAX-DOAS measurements is the system error, and the error of the AMF caused by the ship vibrations is random error. So the error of the AMF calculation caused by the former factors will influence both precision and accuracy of the shipborne MAX-DOAS measurements. For the measurements analyzed in this paper, the errors caused by the uncertainties of the AMF calculation are estimated to be low for most cases with low aerosol loading and good atmosphere conditions.

d. *Spectral analysis and fitting example*

As mentioned in section 3a, the optical density of the measured off-axis and zenith spectra in the same measurement cycle was filtered by a low-order polynomial, representing the slowly varying contribution of broadband absorption, such as the Rayleigh and Mie scattering processes (Ma et al. 2013). The main settings of the DOAS analysis for each trace gas are shown in Table 1. To detect the NO_2 absorption, the cross sections of NO_2 at 293 K (Bogumil et al. 2003), the oxygen dimmer O_4 at 296 K (Greenblatt et al. 1990), Ring spectrum calculated by the DOASIS (Kraus 2001), and the FRS (zenith spectrum in the same measurement cycle, which was used to remove Fraunhofer spectral features and to produce DSCD_{α}) were simultaneously fitted to the atmospheric spectrum between 365 and 390 nm range by the WinDOAS software. As for SO_2 and O_3 retrieval, the cross sections of SO_2 at 293 K (Bogumil et al. 2003), O_3 at

TABLE 1. The main settings of the DOAS analysis for each trace gas.

Retrieved gas	Polynomial order	Fraunhofer reference spectrum	Fitting cross sections	Spectrum region (nm)
NO_2	3	Zenith spectrum of each elevation sequence	NO_2, O_4, Ring (Bogumil et al. 2003)	365–390
SO_2	3	Zenith spectrum of each elevation sequence	SO_2, O_3, Ring (Bogumil et al. 2003)	308–316
O_3	3	Zenith spectrum of each elevation sequence	O_3, SO_2, Ring (Bogumil et al. 2003)	320–330

293 K (Bogumil et al. 2003), Ring spectrum calculated by the DOASIS, and the FRS were simultaneously fitted to the atmospheric spectrum in the 308–316 and 320–330 nm spectral region, respectively, by the WinDOAS software.

With regard to shipborne measurements, the vibrations of the ship can cause the elevation angle error that may influence the AMF calculation. During this shipborne observation campaign, the vibration angle (both roll and pitch) is small ($<\pm2°$) at most times, thanks to the good sea conditions (Fig. 4). Meanwhile, the vibration angles changing between plus and minus signs regularly on the sea in the measurement, which means the total angle error can counteract with each other during the spectra collected time (integrating time, ~1 min). The observational angle change caused by slight vibration was not considered in the paper. With regards to the DOAS retrieval process, other gases such as H_2O and CO_2 were not considered in the fitting procedure due to their weaker absorption in UV and visible spectrum region (360–390 nm) (Du et al. 2013; Schulz et al. 2002; Takashima et al. 2012). Other gases such as NO and HONO were also not considered in the fit procedure because of the lower concentration in the less polluted coastal boundary layer (Stutz et al. 2002).

A fitting example of high NO_2 absorption in the 365–390 nm spectral region (measured spectrum at 5° elevation angle, at 1052 LT 1 September 2014), with NO_2 differential tropospheric slant column density ($DSCD_{\alpha,trop}$) of 11.65×10^{16} molecules cm^{-2}, is shown

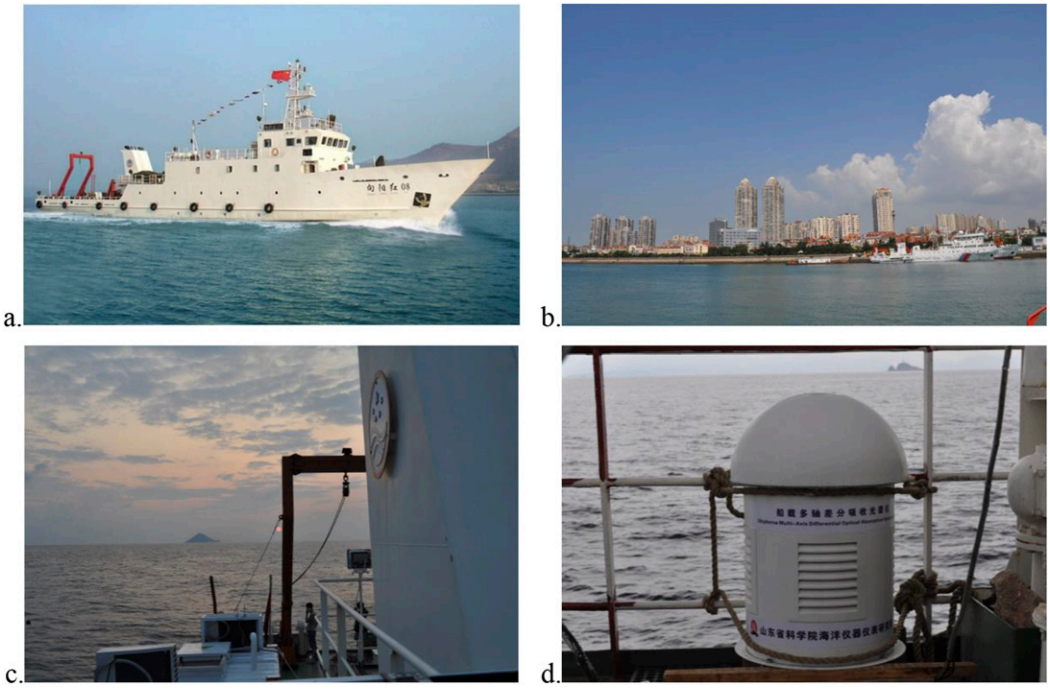

FIG. 4. (a) The *XYH 08*, a Chinese oceanographic research vessel, conducted the shipborne observational campaign. (b) Qingdao coast area monitored by shipborne MAX-DOAS system during the sailing measurements. (c) Sea-condition photo, which is fine during the monitoring time at Dagongdao Island sea area. (d) The working photograph of MAX-DOAS system installed on the portside of the ship.

in Fig. 5. The fit procedure yields the tropospheric differential slant column densities ($DSCD_{\alpha,trop}$) for the atmospheric absorbers by the retrieval method mentioned in section 3b ($DSCD_{\alpha,trop} = SCD_{\alpha} - SCD_{90°}$) (Leser et al. 2003). The red lines in Fig. 5 indicate the reference spectra scaled to the respective absorptions (black lines in Fig. 5) in the measured spectra. At the bottom, the spectral residual (difference between the measured spectra and the fit result) are shown. In this case, the atmospheric NO_2 absorption structure can be clearly extracted from the measured spectra. Cross sections of NO_2, O_4, Ring spectrum, and FRS are included in the fitting procedure.

4. Results and discussion

a. *Time series of NO_2 tropospheric differential slant column density*

As mentioned in section 2b, continuous measurements were performed during the shipborne observation campaign from 30 August to 1 September 2014. The time resolution is decided by the time consuming of spectrum collecting and scanner rotating. The scanner rotating time is constant, and the spectrum collecting time is dependent on the weather condition, which means the spectrum collecting time under clear day is longer than the day of less clouds in order to obtain high-spectra SNR. So the time resolution in our measurement is about 3 min according to the measurement weather condition during a complete MAX-DOAS measurement cycle including 5°, 10°, 20°, and 90° elevation angle observations. Time series of NO_2 tropospheric differential slant column density ($DSCD_{\alpha,trop}$) were calculated with the retrieval method explained in section 3b utilizing the measured spectrum at 5° elevation angle and 90° elevation angle (zenith direction) in the same measurement cycle. As for 5° observation geometry, we can estimate the last scattering altitude (LSA) to be at 1–2 km (or even lower for aerosol load) under Rayleigh scattering and low albedo (<80%) circumstances (Hönninger et al. 2004, their Fig. 8). As a result, the NO_2 $DSCD_{\alpha,trop}$ time series indeed represent the NO_2 level in the boundary layer (BL) of Qingdao offshore sea. Typical time series of NO_2 $DSCD_{\alpha,trop}$ from 30 August to 1 September 2014 during the 1400 to 1530 LT period, are shown in Fig. 6. Error bars denote the SCD fitting errors in the DOAS retrieval process of NO_2 $DSCD_{\alpha,trop}$.

In general, as expected, the $DSCD_{\alpha,trop}$ decreased with increasing elevation angle α in most cases (except for 30 August 2014, due to low NO_2 concentration). On 30 August the *XYH 08* was in the Dagongdao Island sea area (rectangular spot in Fig. 2) and during the time

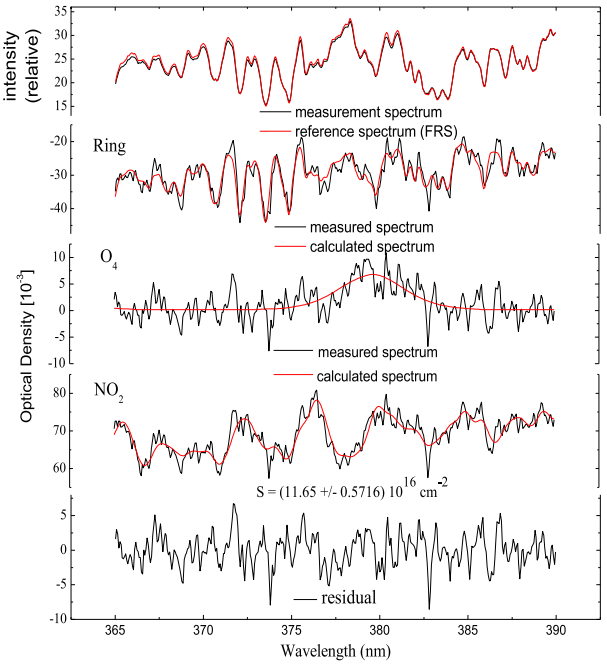

FIG. 5. Example of the NO_2 DOAS evaluation (1052 LT 1 Sep).

period from 1400 to 1530 LT the MAX-DOAS observation direction was toward eastern sea area. The low $DSCD_{\alpha,trop}$ of NO_2 on 30 August 2014 (near zero, Fig. 6a) indicated that the NO_2 content in the BL of the eastern sea area of Dagongdao Island was relatively low. Then we can deduce that the pattern of the NO_2 $DSCD_{\alpha,trop}$ series on 30 August is typical for the Qingdao offshore sea BL, because the air is hardly suffered from pollution except for occasional continental transfer (e.g., result of 31 August). On 31 August the *XYH 08* was also in the Dagongdao Island sea area (rectangular spot in Fig. 2) but during the time period from 1400 to 1530 LT the MAX-DOAS observation direction was toward northeast where the observation area is much more possibly affected by continental transfer if there is northwest wind (Fig. 2 shows the geographic diagram). The high values of NO_2 $DSCD_{\alpha,trop}$ at low elevation angles around 1500 LT showed the occasional presence of pollution in the lower troposphere possibly affected by continental transfer from coastal city because there was northwest wind around 1500 LT on that day. On 1 September the *XYH 08* was in the Jiaozhou Bay sea area (triangle spot in Fig. 2) and during time period from 1400 to 1530 LT the MAX-DOAS observation direction was toward north. As shown in Fig. 6c, the high $DSCD_{\alpha,trop}$ of NO_2 at all elevation angles denote NO_2 abundance due to continental influence and shipping emissions impact. Furthermore, it can be seen from Fig. 6c that the differences in $DSCD_{\alpha,trop}$ at lower

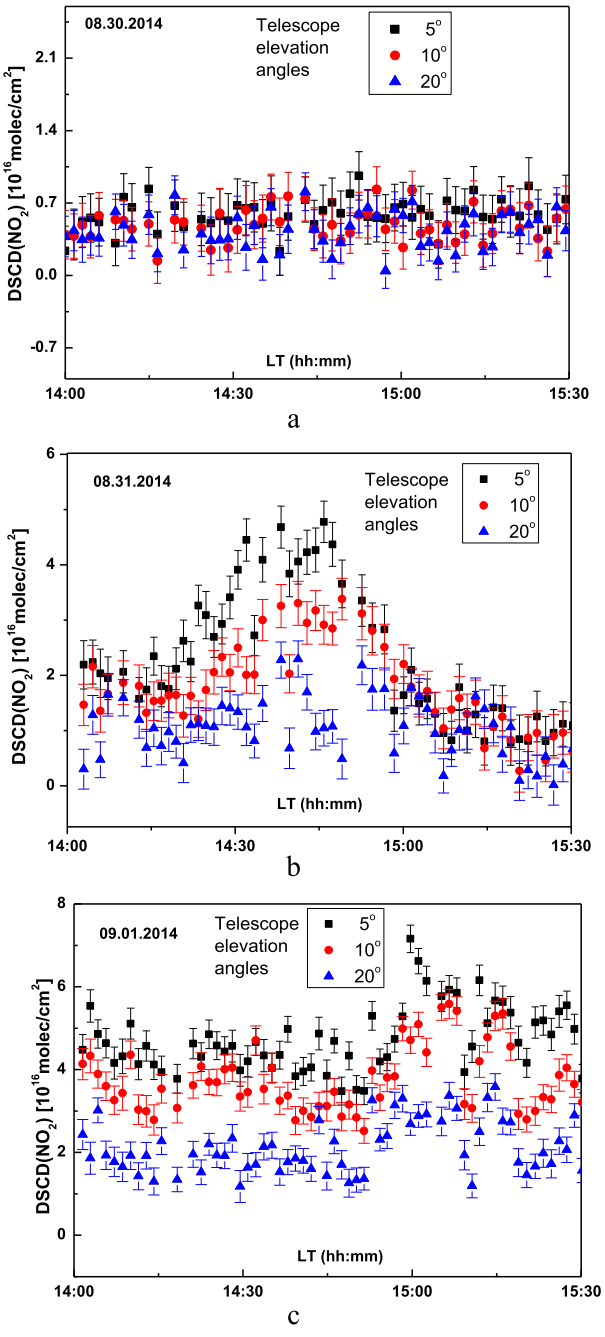

FIG. 6. Typical time series of NO_2 $DSCD_{\alpha,trop}$ during 1400–1530 LT from 30 Aug to 1 Sep 2014 using measurements from the *XYH 08*. Error bars denote SCD fit errors. (a) On 30 Aug, in the Dagongdao Island sea area. (b) On 31 Aug, in the Dagongdao Island sea area. (c) On 1 Sep, in the Jiaozhou Bay sea area.

elevation angles (between 5° and 10°) are small, indicating either high aerosol load or rather constant NO_2 concentration within BL (or both) (Ma et al. 2013).

From Fig. 6c, it is apparent that NO_2 DSCDs increase with decreasing elevation angle due to the high NO_2 levels and different elevation angle observation geometries. It can be seen from Fig. 6 that the temporal variations of the patterns of $DSCD_{\alpha,trop}$ at different elevation angles are mainly similar during the observation periods, which indicates that all elevation angles of the MAX-DOAS observation are highly sensitive to NO_2 in the planetary boundary layer (PBL) (Ma et al. 2013). The $DSCD_{\alpha,trop}$ of NO_2 seems to be higher on heavily polluted area (Jiaozhou Bay, 1 September 2014) than on light polluted area (Dagongdao Island sea, 30 August 2014) during the observation periods. Please note that in this paper we focus on the retrieval of the tropospheric NO_2 VCD from the observations at relatively low elevation angles (5°). The LSA of 5° observation is close to surface, ~1–2 km, under low aerosol load, Rayleigh scattering, and low-albedo circumstances (Hönninger et al. 2004). Under the geometry approximation condition, the effective observation distance (EOD; the farthest distance that the MAX-DOAS can observe) of the MAX-DOAS for NO_2 can be calculated by LSA multiplied by the reciprocal of the sine of the elevation angle (5°). In the case of low aerosol load and low ground albedo, the EOD of the MAX-DOAS for 5° elevation angle is estimated to be ~18 km. The full profile retrieval of trace gases or aerosols (or both) from the shipborne MAX-DOAS observations utilizing all elevation angles will be a subject for further study.

b. *The sailing measurements of NO_2 along the coast of Qingdao*

In the entire duration of the shipborne measurements, there are three sailing periods: one is on the morning of 30 August, from 0800 to 0900 LT; another is on the evening of 31 August, from 1900 to 2000 LT; and the last one is back to port. Because the MAX-DOAS can only make observations during the daytime, sailing measurements were taken just during the first sailing period (the other two-ship sailing period occurred at night). Sailing measurements were started on the morning of 30 August 2014. Instrument was installed on the ship port. Geographic observational directions are shown in Fig. 7 by arrows, which point to Qingdao direction. And the measurements results are presented in Fig. 8.

As mentioned in section 4a, under oversea condition, considered the Rayleigh scattering, the LSA for 5° elevation angle is estimated to be 1–2 km (Hönninger et al. 2004). And for continental condition, considered the larger aerosol load and higher albedo, the LSA for a 5° elevation angle will be less than that under the sea condition (~1 km). During the sailing measurement, the light path between the last scattering place and the MAX-DOAS telescope traveled through the atmosphere above both the offshore sea area and the coastal

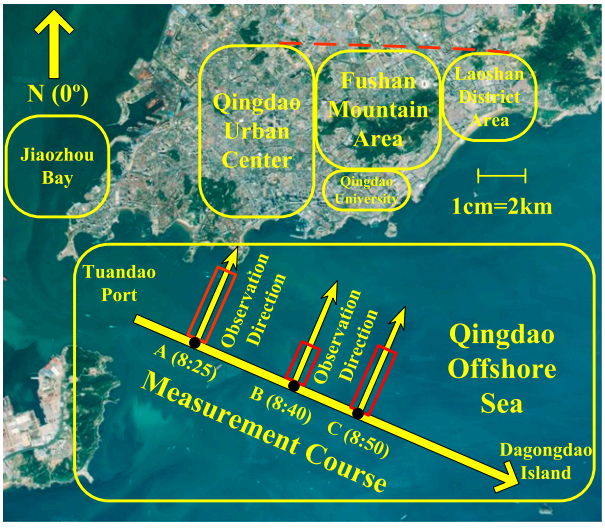

FIG. 7. Geographic diagram of ship sailing measurements on 30 Aug 2014.

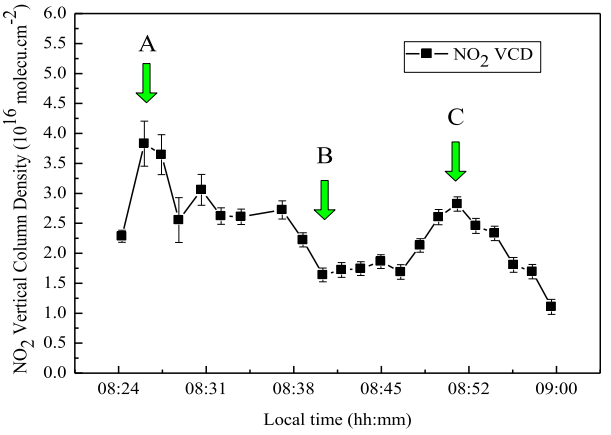

FIG. 8. Result of NO_2 sailing measurements on 30 Aug 2014.

region of Qingdao. Considering the higher aerosol load under the continental condition than under the sea condition, the LSA during the sailing measurement is lower than the LSA of the sea condition, and higher than the LSA of the continental condition. Considering the longer and longer light path over sea at A, B, and C observation points (see Figs. 7 and 8), there will be higher and higher LSA from A to C. According to the EOD calculation there will be longer and longer EOD from A to C. The possible EOD during the sailing measurement was shown by a dashed red line in Fig. 7.

It can be seen from Fig. 8 that at point A (Fig. 7 and 0825 LT) the NO_2 VCD present the maximum value. As shown in Fig. 7, point A is about 6 km away from Qingdao urban center. Due to the high aerosol load and albedo in the Qingdao urban center, as shown by the dashed red line in Fig. 7, the true EOD of the MAX-DOAS would be estimated to be ~12 km, which means the MAX-DOAS observation range can exceed 6 km over the Qingdao urban center (subtracting 6 km oversea distance from the 12 km EOD). It can be deduced that the high NO_2 VCD value revealed the heavy NO_2 pollution in Qingdao urban-center BL (~6 km over urban-center BL). Looking at the monitoring time (0825 LT) and measurement geometry, to a large extent, the traffic emissions (NO_2 from vehicle exhaust gases) during rush hour contribute a lot to the high NO_2 concentration in the Qingdao urban-center BL.

The NO_2 VCD values decrease approaching the Fushan Mountain area. The NO_2 VCD reached the lowest value at point B when the ship arrived at point B (35.9992°N, 120.4155°E,) in Fig. 7 around 0840 LT. At point B in Fig. 7 the MAX-DOAS observation direction pointed toward the Fushan Mountain area (about 8 km far from instrument), which is a mountain located in Qingdao city that is about 5 km long and 380 m in height and covers 7 km^2. As shown by the dashed red line in Fig. 7, the EOD of B place (~14 km) covers the Fushan Mountain area and Qingdao University. The low NO_2 concentration values at point B are probably due to the better air quality in the Fushan Mountain area. As shown in Fig. 8, the concentration of NO_2 increased after point B and it reached a higher value at point C (35.9889°N, 120.4483°E, ~11 km from Laoshan district area) in Fig. 7 at about 0850 LT. Combined by the observation geometry, we can estimate the EOD of C is farther than the other two places (~16 km). As shown by EOD dashed red line in Fig. 7, the MAX-DOAS effective observation distance at point C can cover the Laoshan district (~5 km) where there was heavy traffic in the morning rush hour. Motor vehicle exhaust emission during the morning traffic in Laoshan district may contribute to the higher value of NO_2 measurements results. After point C, the observational direction pointed to Laoshan Mountain area with falling NO_2 concentration results shown in Fig. 8, which indicated better air quality in this area.

c. *Anchor measurements of NO_2, SO_2, and O_3 in the Qingdao offshore sea*

On 1 September the *XYH 08* was anchored inside Jiaozhou Bay (triangular spot in Fig. 2). As shown in Fig. 9, hourly averaged time series of tropospheric trace gas VCD on 1 September 2014 are presented. The overall level of both NO_2 and SO_2 were higher than the other 2 days, which indicated the atmosphere over Jiaozhou Bay may be affected by surrounding traffic or ship emissions. The 8 h backward trajectories of air masses from HYSPLIT ending at 1700 LT

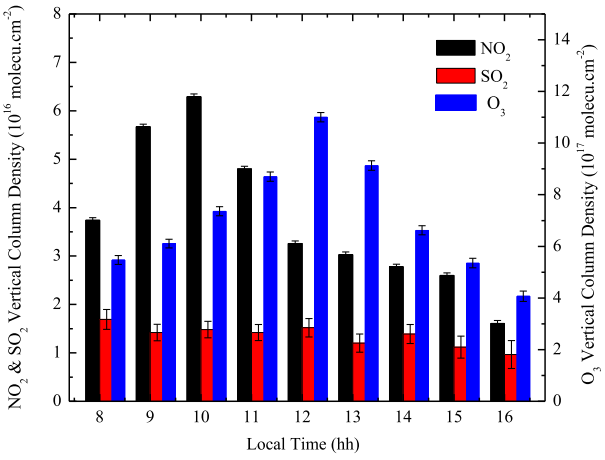

FIG. 9. Hourly average time series of trace gas concentration on 1 Sep 2014.

1 September 2014 are shown in Fig. 10a. It can be seen from the figure that the backward trajectories come from the southeast at 2 km height, which is from the Shinan district of Qingdao city. So the air at the measurement site at 2 km height might suffer from pollution by continental transfer, such as traffic flow and human activity. And the backward trajectories at 4 km height come from the southwest, which is from the Huangdao district and Jiaozhou Bay of Qingdao city. So the air of the measurement site at 4 km height might result from pollution by continental transfer and shipping emissions.

In particular the NO_2 value was high to 6.29×10^{16} molecules cm^{-2} around 1000 LT when the MAX-DOAS observation direction was toward east (~5 km from Qingdao urban area), indicating the high levels of pollution existed in the Qingdao urban area, and decreased in later due to the north MAX-DOAS observation direction (~10 km from the Hongdao suburb coastal area) and the photochemical processes (typical diurnal shape). The overall level of O_3 column density was also high on this day, and it reached the highest value at noon and then gradually declined in the afternoon, which is a typical diurnal shape for tropospheric ozone. The VCDs of SO_2 were relatively low in the observation period compared with the higher VCDs of NO_2. And the VCDs of SO_2 were not significantly affected by the observation direction of the MAX-DOAS indicating the same level of SO_2 between the Qingdao urban area and the Hongdao suburb coastal area on that day.

Daily averaged trace gas concentration time series during the campaign are presented in Fig. 11. From the figure, it can be seen that the overall level of the trace gases on 1 September are all higher than the other 2 days when the *XYH 08* was in the Dagongdao sea area (rectangle in Fig. 2). Specifically, the mean value of NO_2 VCD reached a high value of 3.7×10^{16} molecules cm^{-2}, which is much higher, and 2.7 times of the values of the other 2 days. Likewise, the tropospheric VCDs of SO_2 and O_3 have an increase of 30% and 40%, respectively, on 1 September, compared to the other 2 days, which may be affected by pollution transfer and human activity. The 8 h backward trajectories of air masses from HYSPLIT ending at 1700 LT 30 August 2014 are shown in Fig. 10b. It can be seen from the figure that the backward trajectories come from the open sea under 2 km height, where there is less continental transfer influence for the measurement. The 8 h backward trajectories of air masses from HYSPLIT ending at 1700 LT 31 August 2014 are shown in Fig. 10c. It can be seen that the backward trajectories also come from the open sea under 2 km height, which means there is less continental transfer influence for the measurement. The 8 h backward trajectories of air masses from HYSPLIT are obtained ending at 1700 LT 1 September 2014 in Fig. 10d. It can be seen that the backward trajectories come from east under 2 km height, which there is the center of Qingdao city. It means the air at the measurement site under 2 km height might result from pollution related to continental transfer on 1 September 2014, such as traffic flow or human activity.

The high value of NO_2 on 1 September over Jiaozhou Bay may be affected by the surrounding traffic and shipping emissions. However, the overall levels of NO_2 and SO_2 VCD maintained at 1.0×10^{16} molecules cm^{-2} on 30 and 31 August, which indicate that the contents of the two trace gases in the Dagongdao sea area are relatively low. Note that the shipborne MAX-DOAS measurement site at the first anchor point (35.9602°N, 120.5665°E) is located 6 km southeast of Dagongdao Island (35.969 056°N, 120.502 698°E); the distance from the measurement site to the coast of Qingdao is about 20 km (Fig. 2). So the EOD of shipborne MAX-DOAS at the first anchor point cannot reach the coast of Qingdao. The NO_2 VCD measured in the Dagongdao sea area can represent the level of pollution over the Qingdao offshore area.

d. Comparison with other measurements

Here, we compare the NO_2 VCD measurement results over the Qingdao offshore area with other MAX-DOAS measurements. The tropospheric NO_2 VCDs (in units of 10^{16} molecules cm^{-2}) in different measurements are shown in Table 2 with maximum NO_2 VCD, typical NO_2 VCD, telescope elevation angle (EL), authors, and published year. The EL is the elevation angle of the measured spectrum divided by zenith spectrum in the same cycle to produce DSCD in the tropospheric NO_2 VCD retrieval

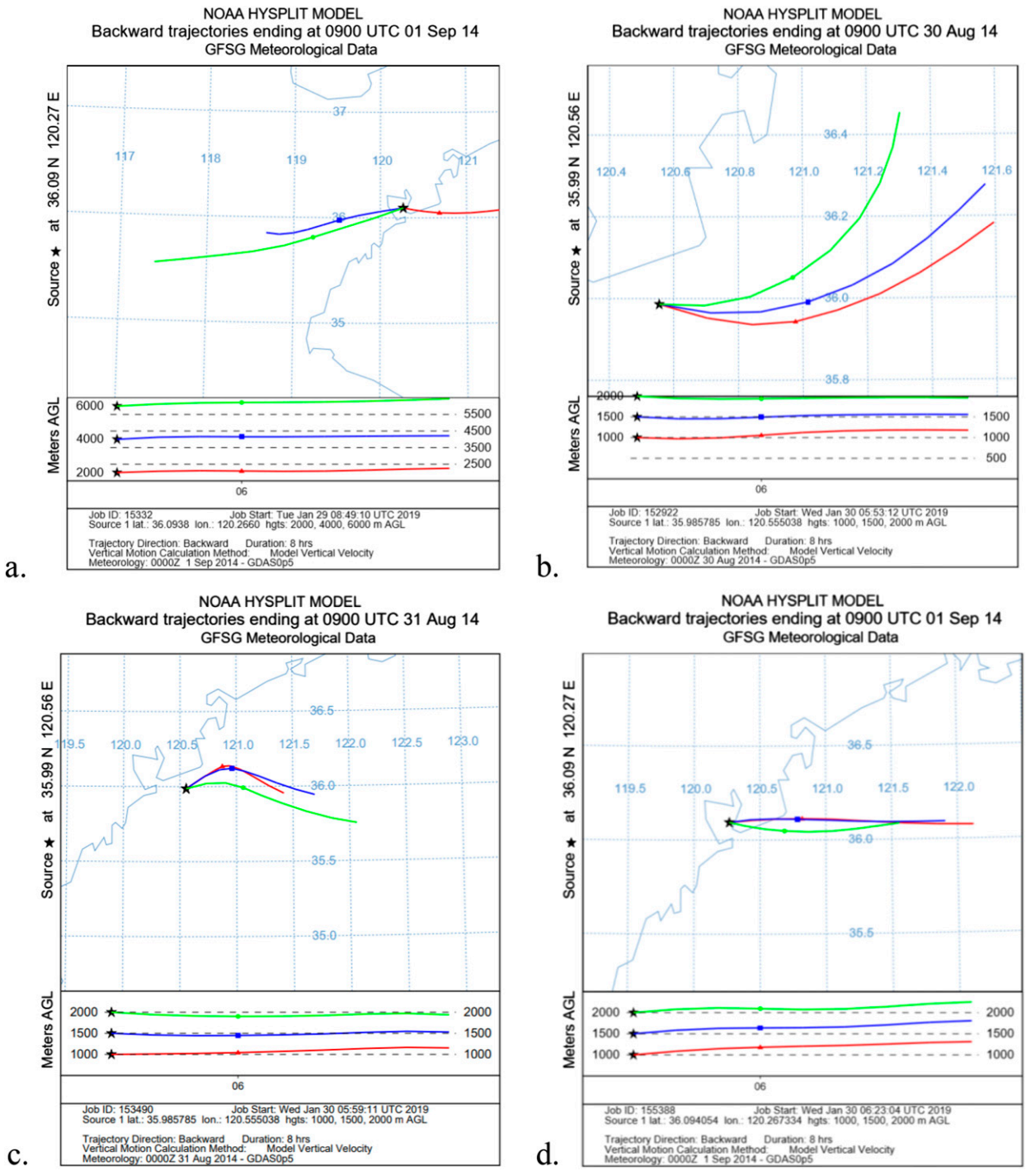

FIG. 10. The backward trajectories of air masses from HYSPLIT at the measurement site during the campaign.

procedure. The EL during the measurement cruise from Bremerhaven, Germany, to Cape Town, South Africa, and over Beijing from 2008 to 2011 was 5° and 30°, respectively. For the measurements over the western Pacific and Indian Oceans and Tai'an from May to June 2006, the specific ELs used during their NO_2 retrieval procedure were not elaborated in the literature but both are at low EL (Table 2).

As shown in Table 2, the shipborne MAX-DOAS measurement cruise from Bremerhaven to Cape Town was made by Leser in October 2000. During the cruise, the NO_2 VCD in the marine boundary layer was measured

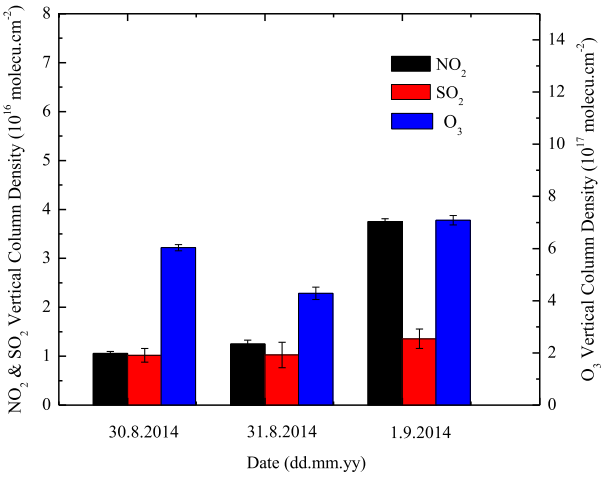

FIG. 11. Daily average concentration of trace gases during the campaign.

at the maximum value of 1.11×10^{16} molecules cm^{-2} over the English Channel, and the typical value of $<0.2 \times 10^{16}$ molecules cm^{-2} was over the remote Atlantic. Because the MAX-DOAS is highly sensitive only to trace gas abundance in the lowest part of the atmosphere, the derived VCDs of 5° EL both in Leser and our measurement are related to a column of 1–2 km height according to the Rayleigh scattering length (Leser et al. 2003). Considering the results mentioned in section 4c, the NO_2 VCD contents in the boundary layer between the English Channel and the Qingdao offshore area were at a comparable level. The shipborne MAX-DOAS measurements of NO_2 VCD near the coast of Japan were made by Takashima in 2012 with a high value of $\sim 9 \times 10^{16}$ molecules cm^{-2}, which was similar with our measurements in Jiaozhou Bay. The tropospheric NO_2 VCD over Tai'an from May to June 2006 and Beijing from 2008 to 2011 were measured by ground-based MAX-DOAS (Irie et al. 2008; Ma et al. 2013). The higher EL of 30° used in the Beijing measurement campaign indicated the relatively higher atmospheric layer observed in the NO_2 VCD measurement than in the other three measurements. Both maximum NO_2 VCD and typical NO_2 VCD were much higher in the Beijing measurement than in the Tai'an measurement campaign, indicating the severe NO_2 pollution in the megacity. The typical NO_2 VCD over the Qingdao offshore area ($\sim 1.0 \times 10^{16}$ molecules cm^{-2}) was in accordance with the case over the Tai'an area and lower than the Beijing measurement.

The 4-month-averaged Ozone Monitoring Instrument (OMI) tropospheric NO_2 VCDs over the measurement site are shown in Fig. 12. The monthly averaged VCDs of the measurement site continued to increase from July to October in 2014. The maximum value happened in the October: $\sim 1.0 \times 10^{16}$ molecules cm^{-2}. Both August and September mean tropospheric NO_2 VCDs were below 1.0×10^{16} molecules cm^{-2} over the measurement site, which were in accordance with our offshore shipborne MAX-DOAS measurement results. But our Jiaozhou Bay measurement results were a little higher than the OMI monthly averaged products. The result bias might come from the monthly averaged satellite data and the different observation mode.

5. Conclusions

The measurements of atmospheric trace gases over a coastal city, Qingdao, have been made by the shipborne MAX-DOAS during a 3-day shipborne observational campaign. Combined with the sailing measurements mode, the shipborne MAX-DOAS can obtain the pollution information of a coastal city along the voyage cruise. It can be found in our sailing measurement results that the traffic emissions played an important part in the BL atmosphere of the coastal city. Moreover, the anchor point measurements showed that the BL trace gases overall level was relatively low in the Qingdao offshore sea, while the level was higher in Jiaozhou Bay, which is located inside the Qingdao district. During the 3-day shipborne observational campaign, the overall levels of NO_2 and SO_2 concentrations maintained at 1.0×10^{16} molecules cm^{-2} offshore, while the NO_2 mean value was about 3.7×10^{16} molecules cm^{-2} for Jiaozhou

TABLE 2. Tropospheric NO_2 VCDs (units of 10^{16} molecules cm^{-2}) in different measurements.

MAX-DOAS measurement	Maximum NO_2 VCD (10^{16} molecules cm^{-2})	Typical NO_2 VCD (10^{16} molecules cm^{-2})	EL	Reference
Measurement cruise from Bremerhaven to Cape Town	1.11 (English Channel)	<0.2 (remote Atlantic)	5°	Leser et al. (2003)
Measurement over the western Pacific and Indian Oceans	~9 (near the coast or in the port of Japan)	<0.1 (over ocean)	<70°	Takashima et al. (2012)
Tropospheric NO_2 VCD over Tai'an (May–June 2006)	1.57	0.94	<90°	Irie et al. (2008)
Tropospheric NO_2 VCD over Beijing (2008–11)	Summer: 13.3 Winter: 16.8	Summer: 3.6 Winter: 5.8	30°	Ma et al. (2013)

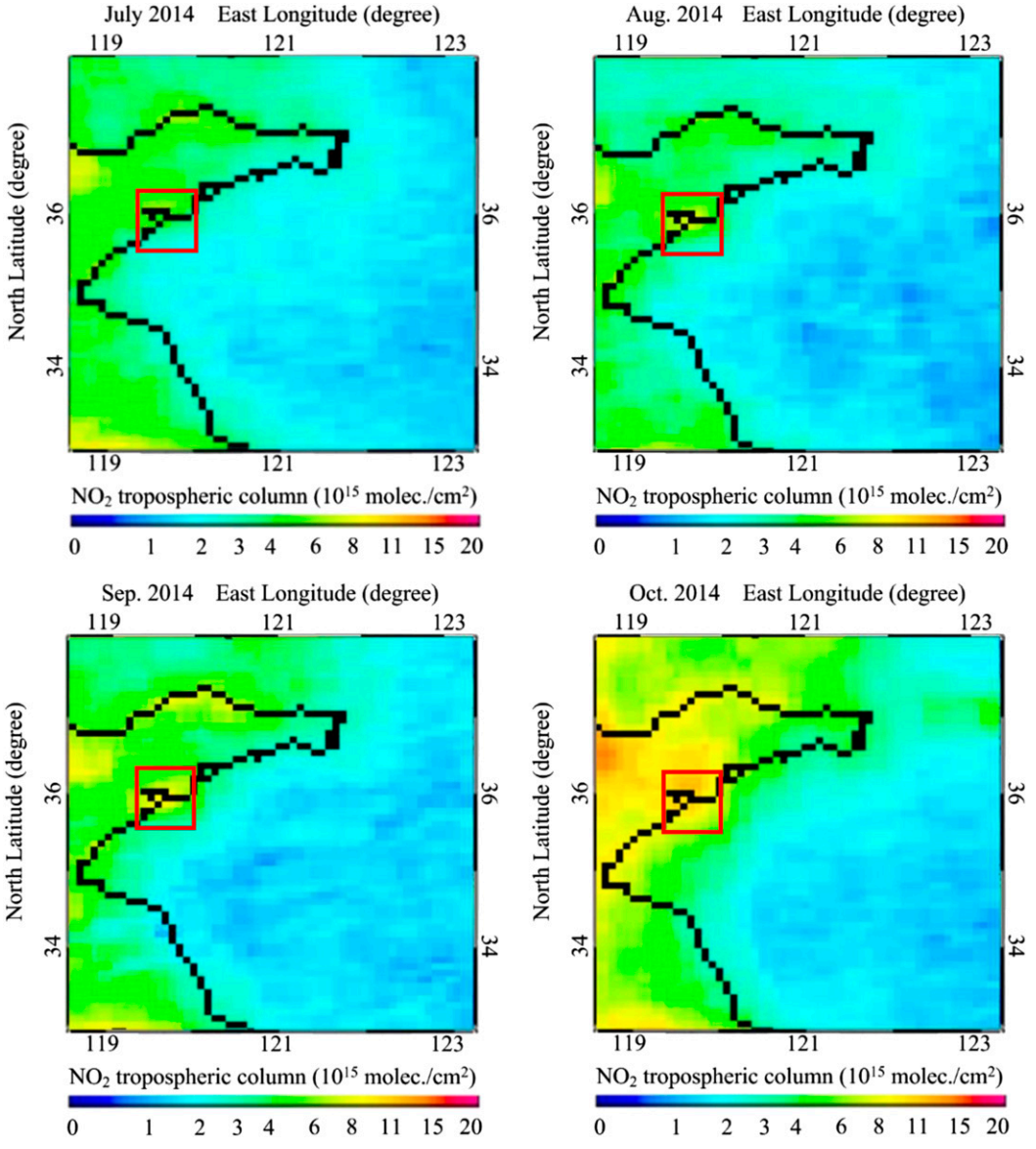

FIG. 12. The monthly averaged OMI tropospheric NO_2 VCDs over the measurement site (red square) for 4 months in 2014 (DOMINO product from TEMIS; see http://www.temis.nl/airpollution/no2.html).

Bay, which was much higher than that offshore. In addition, by comparison with other measurements, our measurement results find good consistency with satellite data and other shipborne MAX-DOAS measurements. In conclusion, we can use the shipborne MAX-DOAS system to monitor multiple trace gas concentrations over a coastal city. Further measurements combining the shipborne MAX-DOAS's advantages in the future may lead to the improved monitoring of trace gases over coastal area.

Acknowledgments. The authors thank the crews of *XYH 08* for their collaboration and efficient navigation during the campaign. The study is funded by the following project grants: 2016YFC1400300, 2018YFC1407300, ZR2017QD009, and 2019GGX104004.

REFERENCES

Bertschi, I. T., R. J. Yokelson, D. E. Ward, T. J. Christian, and W. M. Hao, 2003: Trace gas emissions from the production and use of domestic biofuels in Zambia measured by open-path Fourier transform infrared spectroscopy. *J. Geophys. Res.*, **108**, 8469, https://doi.org/10.1029/2002JD002158.

Bevington, P. R., and D. K. Robinson, 1992: *Data Reduction and Error Analysis for the Physical Sciences*. McGraw-Hill, 328 pp.

Bobrowski, N., G. Honninger, B. Galle, and U. Platt, 2003: Detection of bromine monoxide in a volcanic plume. *Nature*, **423**, 273–276, https://doi.org/10.1038/nature01625.

Bogumil, K., and Coauthors, 2003: Measurements of molecular absorption spectra with the SCIAMACHY pre-flight model: Instrument characterization and reference data for atmospheric remote-sensing in the 230–2380 nm region. *J. Photochem. Photobiol. Chem.*, **157**, 167–184, https://doi.org/10.1016/S1010-6030(03)00062-5.

Bortoli, D., A. M. Silva, M. J. Costa, A. F. Domingues, and G. Giovanelli, 2009a: Measurements of stratospheric ozone and nitrogen dioxide at Èvora, Portugal. *Int. J. Remote Sens.*, **30**, 4209–4226, https://doi.org/10.1080/01431160902822849.

——, ——, ——, ——, and ——, 2009b: Monitoring of atmospheric ozone and nitrogen dioxide over the south of Portugal by ground-based and satellite observations. *Opt. Express*, **17**, 12944, https://doi.org/10.1364/OE.17.012944.

Du, J., L. Huang, Q.-L. Min, and L. Zhu, 2013: The influence of water vapor absorption in the 290–350 nm region on solar radiance: Laboratory studies and model simulation. *Geophys. Res. Lett.*, **40**, 4788–4792, https://doi.org/10.1002/grl.50935.

Edner, H., P. Ragnarson, S. Svanberg, and E. Wallinder, 1994: Total fluxes of sulfur dioxide from the Italian volcanoes Etna, Stromboli, and Vulcano measured by differential absorption lidar and passive differential optical absorption spectroscopy. *J. Geophys. Res.*, **99**, 18 827–18 838, https://doi.org/10.1029/94JD01515.

Galle, B., C. Oppenheimer, A. Geyer, A. J. S. McGonigle, M. Edmonds, and L. Horrocks, 2003: A miniaturised ultraviolet spectrometer for remoter sensing of SO_2 fluxes: A new tool for volcano surveillance. *J. Volcanol. Geotherm. Res.*, **119**, 241–254, https://doi.org/10.1016/S0377-0273(02)00356-6.

Greenblatt, G. D., J. J. Orlando, J. B. Burkholder, and A. R. Ravishankara, 1990: Absorption measurements of oxygen between 330 and 1140 nm. *J. Geophys. Res.*, **95**, 18 577–18 582, https://doi.org/10.1029/JD095iD11p18577.

Heckel, A., A. Richter, T. Tarsu, F. Wittrock, C. Hak, I. Pundt, W. Junkermann, and P. J. Burrows, 2005: MAX-DOAS measurements of formaldehyde in the Po-Valley. *Atmos. Chem. Phys.*, **5**, 909–918, https://doi.org/10.5194/acp-5-909-2005.

Hendrick, F., and Coauthors, 2006: Intercomparison exercise between different radiative transfer models used for the interpretation of ground-based zenith-sky and multi-axis DOAS observations. *Atmos. Chem. Phys.*, **6**, 93–108, https://doi.org/10.5194/acp-6-93-2006.

Hönninger, G., V. C. Friedeburg, and U. Platt, 2004: Multi axis differential optical absorption spectroscopy (MAX-DOAS). *Atmos. Chem. Phys.*, **4**, 231–254, https://doi.org/10.5194/acp-4-231-2004.

Irie, H., Y. Kanaya, H. Akimoto, H. Tanimoto, Z. Wang, J. F. Gleason, and E. J. Bucsela, 2008: Validation of OMI tropospheric NO_2 column data using MAX-DOAS measurements deep inside the North China Plain in June 2006: Mount Tai Experiment 2006. *Atmos. Chem. Phys.*, **8**, 6577–6586, https://doi.org/10.5194/acp-8-6577-2008.

Johansson, M., B. Galle, T. Yu, L. Tang, D. Chen, H. Li, J. X. Li, and Y. Zhang, 2008: Quantification of total emission of air pollutants from Beijing using mobile mini-DOAS. *Atmos. Environ.*, **42**, 6926–6933, https://doi.org/10.1016/j.atmosenv.2008.05.025.

Khalil, M. A. K., and R. A. Rasmussen, 1990: Patterns of trace gases near sources of global pollution. *J. Air Waste Manage. Assoc.*, **40**, 1143–1146, https://doi.org/10.1080/10473289.1990.10466760.

Kraus, S., 2001: DOASIS, DOAS for Windows software. *Proc. First Int. DOAS Workshop*, Heidelberg, Germany, University of Heidelberg.

Leigh, R. J., G. K. Corlett, U. Friess, and S. P. Monks, 2006: Concurrent multiaxis differential optical absorption spectroscopy system for the measurement of tropospheric nitrogen dioxide. *Appl. Opt.*, **45**, 7504–7518, https://doi.org/10.1364/AO.45.007504.

Leser, H., G. Honninger, and U. Platt, 2003: MAX-DOAS measurements of BrO and NO_2 in the marine boundary layer. *Geophys. Res. Lett.*, **30**, 1537, https://doi.org/10.1029/2002GL015811.

Ma, J. Z., S. Beirle, J. L. Jin, R. Shaiganfar, P. Yan, and T. Wagner, 2013: Tropospheric NO_2 vertical column densities over Beijing: Results of the first three years of ground-based MAX-DOAS measurements (2008-2011) and satellite validation. *Atmos. Chem. Phys.*, **13**, 1547–1567, https://doi.org/10.5194/acp-13-1547-2013.

Machida, T., and Coauthors, 2008: Worldwide measurements of atmospheric CO_2 and other trace gas species using commercial airlines. *J. Atmos. Oceanic Technol.*, **25**, 1744–1754, https://doi.org/10.1175/2008JTECHA1082.1.

Platt, U., 1994: Differential optical absorption spectroscopy (DOAS), air monitoring by spectroscopic techniques. *Chem. Anal. Ser.*, **127**, 27, https://doi.org/10.1002/9780470027318.A0706.

——, and J. Stutz, 2008: *Differential Optical Absorption Spectroscopy: Principles and Applications*. Springer, 597 pp.

Premuda, M., S. Masieri, D. Bortoli, I. Kostadinov, A. Petritoli, and G. Giovanelli, 2011: Evaluation of vessel emissions in a lagoon area with ground based multi axis DOAS measurements. *J. Atmos. Environ.*, **45**, 5212–5219, https://doi.org/10.1016/j.atmosenv.2011.05.067.

Press, W. H., S. A. Teukolsky, W. T. Vetterling, and B. P. Flannery, 1992: *Numerical Recipes in C: The Art of Scientific Computing*. 2nd ed. Cambridge University Press, 994 pp.

Rozanov, A., V. Rozanov, M. Buchwitz, A. Kokhanovsky, and J. P. Burrows, 2005: SCIATRAN 2.0—A new radiative transfer model for geophysical applications in the 175–2400 nm spectral region. *Adv. Space Res.*, **36**, 1015–1019, https://doi.org/10.1016/j.asr.2005.03.012.

Sanders, R. W., S. Sloomon, J. P. Smith, L. Perliski, H. L. Miller, G. H. Mount, J. G. Keys, and A. L. Schmeltekopf, 1993: Visible and near-ultraviolet spectroscopy at McMurdo Station, Antarctica: 9. Observations of OClO from April to October 1991. *J. Geophys. Res.*, **98**, 7219–7228, https://doi.org/10.1029/93JD00042.

Schempp, H., S. Hippeli, E. F. Elstner, and C. Langebartels, 2004: Air pollution: Trace gases as inducers of plant damage. *Plant Toxicology*, B. Hock and E. F. Elstner, Eds., Marcel Dekker, 151–190.

Schulz, C., J. D. Koch, D. F. Davidson, J. B. Jeffries, and R. K. Hanson, 2002: Ultraviolet absorption spectra of shock-heated carbon dioxide and water between 900 and 3050 K. *Chem. Phys. Lett.*, **355**, 82–88, https://doi.org/10.1016/S0009-2614(02)00190-2.

Stutz, J., B. Alicke, and A. Neftel, 2002: Nitrous acid formation in the urban atmosphere: Gradient measurements of NO_2 and HONO over grass in Milan, Italy. *J. Geophys. Res.*, **107**, 8192, https://doi.org/10.1029/2001JD000390.

Takashima, H., H. Irie, Y. Kanaya, and F. Syamsudin, 2012: NO_2 observations over the western Pacific and Indian Ocean by MAX-DOAS on *Kaiyo*, a Japanese research vessel. *Atmos. Meas. Tech.*, **5**, 2351–2360, https://doi.org/10.5194/amt-5-2351-2012.

Wagner, T., O. Ibrahim, R. Shaiganfar, and U. Platt, 2010: Mobile MAX-DOAS observations of tropospheric trace gases. *Atmos. Meas. Tech.*, **3**, 129–140, https://doi.org/10.5194/amt-3-129-2010.

Weibring, P., H. Edner, S. Svanberg, G. Cecchi, L. Pantani, R. Ferrara, and T. Caltabiano, 1998: Monitoring of volcanic sulphur dioxide emissions using differential absorption lidar (DIAL), differential optical absorption spectroscopy (DOAS), and correlation spectroscopy (COSPEC). *Appl. Phys.*, **67B**, 419–426, https://doi.org/10.1007/s003400050525.

——, J. Swartling, H. Edner, S. Svanberg, T. Caltabiano, D. Condarelli, G. Cecchi, and L. Pantani, 2002: Optical monitoring of volcanic sulphur dioxide emissions—Comparison between four different remote-sensing spectroscopic techniques. *Opt. Lasers Eng.*, **37**, 267–284, https://doi.org/10.1016/S0143-8166(01)00084-7.

Wittrock, F., H. Oetjen, A. Richter, S. Fietkau, T. Medeke, A. Rozanov, and J. P. Burrows, 2003: MAX-DOAS measurements of atmospheric trace gases in Ny-Alesund. *Atmos. Chem. Phys.*, **3**, 6109–6145, https://doi.org/10.5194/acpd-3-6109-2003.